Optical properties of molybdenum. I. Experiment and Kramers-Kronig analysis*

B. W. Veal and A. P. Paulikas
Argonne National Laboratory, Argonne, Illinois 60439
(Received 19 February 1974)

A study of the optical properties and electronic structure of molybdenum is reported in a two-paper experimental and theoretical series. Reflectivity data between 0.5 and 6 eV are presented, and Kramers-Kronig analytical procedures used to determine the optical functions $\epsilon_1(\omega)$ and $\epsilon_2(\omega)$ are discussed. Procedures are discussed for obtaining suitable extrapolations of $R(\omega)$ in the ranges $\omega_{min} \to 0$ and $\omega_{max} \to \infty$. (ω_{min} and ω_{max} are the energy extremes of the measured spectral range.) A new method (for metals) is presented for optimizing the extrapolation $R(\omega)$ in the range $\omega_{min} \to 0$. Recently reported sum rules are evaluated to test the inversion procedures.

I. INTRODUCTION

In this two-paper series we present a study of the optical properties of molybdenum and their relation to the electronic structure. In paper I we report near-normal-incidence reflectance measurements taken between 0.5 and 6.0 eV and the determination of the complex dielectric function $\hat{\epsilon} = \epsilon_1 + i\epsilon_2$ obtained by Kramers-Kronig inversion of the reflectance data. In paper II, $\epsilon_2(\omega)$ is examined within the context of one-electron theory. Specifically, a new relativistic-augmented-plane-wave (RAPW) band calculation is presented from which $\epsilon_2(\omega)$ is computed within the framework of both direct and indirect interband transition models.

Whereas a number of measurements of the optical constants[1-14] have been reported for molybdenum below 6 eV, substantial disagreement is found between the reported results of the different investigators. To illustrate, the magnitudes of the reported reflectivities vary by as much as 0.3 (at least 40% of the measured reflectivity) at 5 eV and the uncertainties in the optical constants are correspondingly large. Surprisingly, among the lowest-reported reflectivities are data presented in Ref. 12 which were taken on samples prepared and measured in high vacuum (10^{-10}-Torr range). However, optical-reflectance studies of chemisorption on clean molybdenum surfaces[15] have shown that, between 2 and 5 eV, the reflectivity *decreases* a small amount with *increasing* oxygen adsorption. Thus it does not appear that the large discrepancies in the literature result from surface oxidation (at least with bulk sample studies) but more likely from a combination of experimental difficulties. Our reflectivity measurements, taken under a variety of surface preparation conditions, are generally consistent with Refs. 1–5 and are in good agreement with the recently reported absorptivity data of Ref. 6 taken at cryogenic temperatures. The experimental procedures are discussed in Sec. II.

Since the Kramers-Kronig inversion requires the evaluation of integrals over an infinite spectral range, extrapolations of the reflectance are needed for ω both larger and smaller than the measured data range. A nearly unique extrapolation procedure appropriate to metals was developed for the spectral range $\omega_{min} \to 0$ where ω_{min} is the lowest-energy datum point measured. By including the dc conductivity as a datum point, the inversion procedure yields the remaining Drude parameter τ, the mean-electron scattering time. This extrapolation procedure, as well as the procedure for doing the $\omega \to \infty$ extrapolation, is discussed in Sec. III. An example is presented to illustrate that unknown structure outside the measured spectral range has a minimal effect on the inverted results within the measured range. In Sec. IV, we present computations of several sum-rule integrals.

II. EXPERIMENTAL

Samples were prepared from at least 0.9999-pure Mo cut from both single (unknown orientation) and polycrystalline ingots. After cutting, lapping, and mechanical polishing (final finish with 3-μm diamond grit), the samples were electropolished to remove any residual surface damage or contamination. Three electropolishing solutions were used, all of which produced reasonably specular surfaces. The solutions, polishing conditions and the estimated surface removal are listed in Table I. After electropolishing, sample III was subsequently sputtered for 1 h at 1000 V in an argon-glow discharge at 50 μ argon pressure. After sputter etching, the sample was transferred to the reflectometer with a vacuum-capping procedure designed to prevent exposing the sample to air. Measurements were then taken with the sample in an ion-pumped vacuum system at $\sim 5 \times 10^{-7}$ Torr.

TABLE I. Sample electropolishing conditions.

Sample	Electropolish	Cathode	Temp. (°C)	Estimated current density (A/cm^2)	Time (min)	Amount removed[a] (μ)
III (large-grain polycrystal)	85% H_2SO_4, 15% HF	platinum	25	0.5	1.5	20
IV (small-grain polycrystal)	68% H_3PO_4, 15% H_2SO_4 17% H_2O	Stainless steel	60	1	2	10
V (single crystal)	1 part H_2SO_4, 7 parts methanol	platinum	15	1	2	50

[a] As determined by loss of weight.

Sample IV was also electropolished and sputtered but was measured in air. Sample V was simply electropolished with no ion etching and was also measured in air. The electropolishing and ion sputtering left the surface rather rough and wavy with the result that some light was lost from the reflected beam. In order to compensate for the roughness-dependent light loss, a film overcoating procedure[16] accurate to about 2% was used. With the exception of sample IV, all results were reproducible within this accuracy. For sample IV, a noticeable dropoff occurred in the measured reflectivity above ~4.2 eV although for lower energies the results were indistinguishable within experimental error from the other samples. The reflecting surface of sample IV was prepared from an ingot which was cold worked and subsequently strain relieved (15 min at 920°C) to produce extremely fine grains. It may be that the sample contained residual cold work or that etching of the fine-grain structure produced a microroughness favorable for the excitation of surface plasmons.[17] The reflectance of samples with microrough surfaces will show increased attenuation (relative to smooth surfaces)[17,18] when ϵ_1 of the bulk material is approximately equal to -1. Since ϵ_1 is apparently small and negative over much of the range between 1 and 15 eV,[1-13] the probability of surface-plasmon excitation in Mo for $E < 6$ eV for appropriately rough surfaces would be high. Because of the possibility of anomalous surface-dependent behavior, the data for sample IV were not Kramers-Kronig analyzed. Figure 1 shows the measured reflectivity for molybdenum (sample V) taken between 0.2 and 6 eV.

Precision of at least one part in 10^4 was available for energies greater than ~1.5 eV, but the precision dropped to approximately 5 parts in 10^3 at 0.5 eV. Data points were taken at 0.05-eV intervals or less with a spectrometer bandpass of 0.02 eV or less. Thus, for energies greater than ~1 eV, data were available at sufficiently high precision and density to justify numerical differentiation. Since the precision in R is preserved in the inverted ϵ_2, the energy derivative $d(E^2\epsilon_2)/dE$ was calculated and can be seen in Fig. 6 of paper II.

III. KRAMERS-KRONIG INVERSION

A. Analytical procedure

The reflectivity data were Kramers-Kronig inverted to obtain the components of the complex dielectric function

$$\hat{\epsilon} = \epsilon_1 + i\epsilon_2 . \tag{1}$$

The inversion procedure involves the calculation of the phase

$$\theta(\omega) = \frac{\omega}{\pi} P \int_0^\infty \frac{\ln R(\omega')d\omega'}{\omega^2 - \omega'^2} \tag{2}$$

from the measured reflectivity $R(\omega')$. The complex dielectric function is then computed from Fresnel's relation

$$\hat{\epsilon}(\omega) = \left(\frac{1+\hat{r}(\omega)}{1-\hat{r}(\omega)}\right)^2 , \tag{3}$$

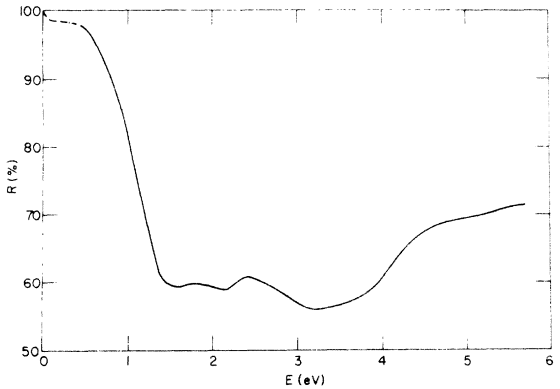

FIG. 1. Measured reflectance of molybdenum between 0.5 and 6 eV.

where the complex reflectivity is defined as

$$\hat{r}(\omega) = [R(\omega)]^{1/2} e^{i\theta(\omega)} . \tag{4}$$

Equation (2) is an infinite integral and, of course, data are available for a restricted energy range. Thus a procedure is needed to extrapolate $R(\omega)$ toward both zero and infinite frequencies.

To carry out the Kramers-Kronig inversion, the following procedure was used: Let us represent $\ln R(\omega)$ as the sum[16]

$$\ln R(\omega) = \ln A(\omega) + \ln B(\omega) . \tag{5}$$

Now let us assume that $A(\omega)$ represents the reflectivity of a collection of harmonic-oscillator absorbers. We have[19]

$$A(\omega) = \hat{r}^*(\omega)\hat{r}(\omega) , \tag{6}$$

where

$$\hat{r}(\omega) = \frac{[\hat{\epsilon}(\omega)]^{1/2} - 1}{[\hat{\epsilon}(\omega)]^{1/2} + 1} \tag{7}$$

and

$$\hat{\epsilon}(\omega) = 1 + \sum_{j=1}^{n} \frac{f_j}{(\omega_j^2 - \omega^2) - i\Gamma_j\omega} , \tag{8}$$

with phase

$$\theta(\omega) = \arctan\left(\frac{\mathrm{Im}\,\hat{r}}{\mathrm{Re}\,\hat{r}}\right) , \tag{9}$$

where n is the number of harmonic-oscillator absorbers located at positions ω_j; Γ_j represents a broadening parameter.

The parameters of Eq. (8) are chosen so that $A(\omega_{\max}) = R(\omega_{\max})$, where $\omega_{\max}$ is the high-energy extreme of the data range. (Also, we define $\omega_{\min}$ as the lowest-measured energy). If we allow the model function (8) to provide the high-energy extrapolation, we see from Eqs. (2) and (5),

$$\theta(\omega) = \frac{\omega}{\pi} P\int_0^{\infty} \frac{\ln A(\omega')\,d\omega'}{\omega^2 - \omega'^2} + \frac{\omega}{\pi} P\int_0^{\infty} \frac{\ln B(\omega')}{\omega^2 - \omega'^2}\,d\omega'$$

$$= \theta_m(\omega) + \frac{\omega}{\pi} P\int_0^{\omega_{\max}} \frac{[\ln R(\omega') - \ln A(\omega')]\,d\omega'}{\omega^2 - \omega'^2} . \tag{10}$$

We have now separated $\theta(\omega)$ into two terms, an integral which need be evaluated only for energies less than $\omega_{\max}$ [since $R(\omega)$ is assumed equal to $A(\omega)$ above $\omega_{\max}$] and a term $\theta_m(\omega)$ which is readily computed from Eq. (9). The integral of Eq. (10) is then evaluated with the integration program developed by Kreiger *et al.*[20]

This inversion procedure has proven to be particularly satisfactory since the calculation can be performed with a minimum of computer time (~10 sec of machine time on the IBM 360/75/195 is needed to evaluate $\hat{\epsilon}$ at 500 energies from 500 input-reflectivity datum points) and it provides a natural extrapolation function with the correct[21] $R \propto 1/\omega^4$ dependence at high frequencies. Also, very weak spectral structure found in $R(\omega)$ will be preserved in the inverted $\hat{\epsilon}$. This feature is particularly useful when high-precision-reflectance data are available. (Such a capability would not generally be available for inversion routines which require functional fitting[22-24] to experimental data since fitting errors would appear as spurious weak structures in $\hat{\epsilon}$.)

For performing Kramers-Kronig inversions, the principal computation difficulty rests with the fact that Eq. (2) is a principal-value integral which normally has the largest contribution to $\theta(\omega)$ when the variable of integration ω' is near the singular point ω. It has been our experience that use of the integration routine[20] alone provides satisfactory results at relatively low energies (below ~15 eV) but becomes increasingly unsatisfactory for calculations at higher energies as evidenced by increasingly anomalous behavior of $\theta(\omega)$. However, with the procedure outlined above, integration is needed merely to provide a perturbation-type correction on the model-function reflectivity only within the measured data range. The procedure has been verified by inverting reflectivities calculated from a variety of harmonic-oscillator model functions.

B. Extrapolation $\omega \to \infty$

For the $\omega \to \infty$ extrapolation, we have found that it is always adequate to represent Eq. (8) with a single Drude-like absorber; that is, with $n = 1$ and $\omega_1 = 0$. The two parameters f_1 and Γ_1 are then chosen to match the magnitude of the experimental $R(\omega_{\max})$ and to scale the resultant Kramers-Kronig inverted $\hat{\epsilon}(\omega)$. Our experimental measurements (to 5.6 eV) were extended to 25 eV with the data of Juenker *et al.*[5] (see Fig. 2, curve A) and were extrapolated beyond that point with the two-parameter function discussed above using $f_1 = 600$ eV^2 and $\Gamma_1 = 7.622$ eV^{-1} where ω is expressed in eV.

However, if we had chosen to ignore the Juenker *et al.* data, we could use the two-parameter extrapolation starting at 5.6 eV (Fig. 2, curve B). If these extrapolation parameters are carefully chosen, we find that the Kramers-Kronig inverted results (below 5.6 eV) are nearly indistinguishable from the results of the previous inversion which made use of experimental data between 0 and 25 eV. These results for the frequency-dependent conductivity $\sigma(\omega)$ are shown in Fig. 3 where the

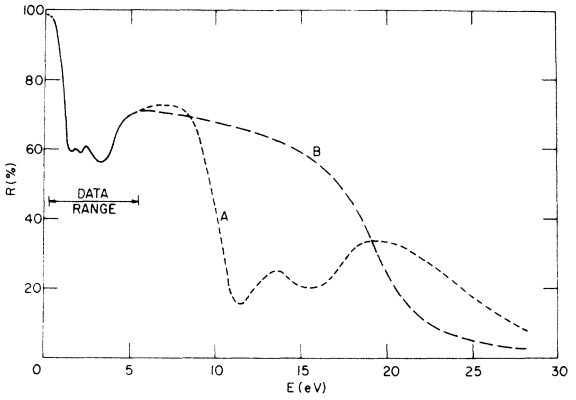

FIG. 2. Extrapolation functions (dashed lines) used for Kramers-Kronig inversion of the measured reflectance (solid line) obtained below 6 eV. Curve A was taken from Ref. 5 and Curve B is a Drude-type model function.

solid line was obtained making use of the 0–25-eV data and the diamond-shaped points were obtained from the inversion of data extrapolated with a model function above 5.6 eV. We see that these results are essentially identical for the entire data range. This illustrates that structure in $R(\omega)$ which might appear outside the data range is a matter of little consequence to the inverted results within the data range. We must emphasize, however, that the magnitude of $\sigma(\omega)$ within the data range is strongly dependent on the choice of extrapolation function. Thus one might decide upon an alternate extrapolation procedure, namely of choosing the parameters f_1 and Γ_1 in order to match $R(\omega_{max})$ and to scale $\sigma(\omega)$ at some $\omega = \omega_0$ to some independently measured $\sigma(\omega_0)$. In Fig. 3, for example, we also show (open circles) data reported by Kirillova *et al.*[1] for samples measured ellipsometrically in air. In Fig. 4, we show Kirillova's results along with the inverted $\sigma(\omega)$ obtained with an extrapolation (from 5.6 eV to ∞) which scales σ to Kirillova's results at 2.3 eV. These data are in generally satisfactory agreement but show significant differences, particularly for $E \lesssim 1$ eV. Unlike normal incidence-reflectance data, ellipsometric data are very sensitive to thin films which might be adsorbed on the sample surface. Since the ellipsometric measurements were taken in air, surface-film contaminants could seriously affect the reported results. Of course, uncertainties in the measured reflectivities and in the Kramers-Kronig inversion can also account for some of the difference between the ellipsometric results and the inverted results of Fig. 3. We note parenthetically that normal incidence-reflectance measurements are simpler, are less sensitive to sample contamination, and generally afford higher precision than ellipsometry. Nonetheless, ellipsometry provides a direct measure of $\sigma(\omega)$. As we have seen, even a single $\sigma(\omega)$ point which is accurately known will enable one to perform accurate Kramers-Kronig inversion of reflectivity data even though the data are available over a very limited spectral range. A few carefully acquired ellipsometric measurements used in combination with normal incidence-reflectivity data can thus provide a powerful measurement technique.

For the purposes of subsequent analyses (particularly for the succeeding paper II of this study) we will use the results of the inversion given by the solid line of Fig. 3. That is, the result de-

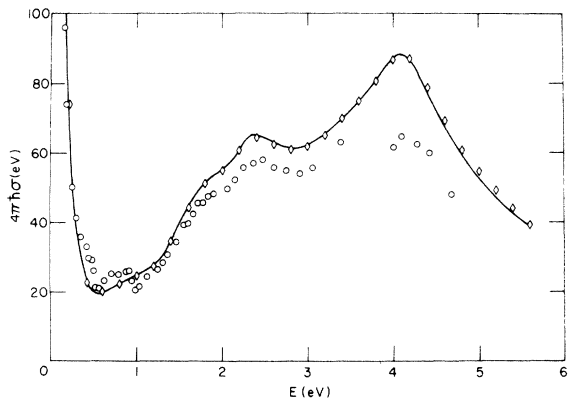

FIG. 3. Measured frequency-dependent conductivity below 6 eV. The solid line was obtained from Kramers-Kronig inversion of the measured reflectance using extrapolation A of Fig. 2; the diamond points using extrapolation B of Fig. 2. This figure illustrates that unknown structures outside the measured spectral range need not seriously affect the inverted optical functions within the measured range. The circles are from Ref. 1.

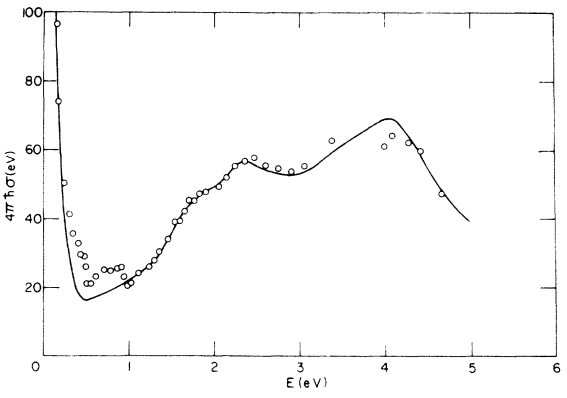

FIG. 4. $\sigma(\omega)$ (solid line) obtained using a Drude-type extrapolation with extrapolation parameters chosen to satisfy the conditions $R(\omega_{max})_{calc} = R(\omega_{max})_{exptl}$ and $\sigma(\omega) = \sigma(\omega)_k$ at 2.3 eV, where $\sigma(\omega)_k$ (circles) are the results of Ref. 1.

rived exclusively from near-normal-incidence-reflectance measurements.

C. Extrapolation $\omega \to 0$

The inverted $\sigma(\omega)$ within the data range shows some sensitivity to the $\omega \to 0$ reflectance extrapolation. However, it appears that a self-consistency condition is available within the Kramers-Kronig formalism so that an optimum extrapolation function for the $\omega_{\min} \to 0$ region can be obtained. We shall impose the conditions that (a) $\sigma(\omega)$ obey a Drude expression over the maximum possible energy range (consistent with the data) for $\omega > 0$ and (b) $\sigma(0)$ be equal to the bulk dc conductivity σ_{dc}; i.e., we shall regard σ_{dc} as a legitimate datum point. [If prominent structure resulting from the anomalous skin effect appears in $R(\omega)$, our extrapolation procedure may be invalid. However, the work of Bennett *et al.*[25] on silver shows that for reasonably smooth sample surfaces, the anomalous skin effect has a minor effect on room-temperature reflectance measurements. Also, low-energy interband transitions or frequency dependence of the electron scattering time may mean that, for this analysis, data are needed to very small ω.]

The rationale for condition (a) is based on the argument that, at some sufficiently small ω, $\sigma(\omega)$ should become Drude-like. Hopefully, experimental data would be available at sufficiently low ω where interband absorption would be negligible. In the absence of sufficiently low ω data, however, there is little point in speculating on the possible interband absorption below $\omega_{\min}$. Instead, it would seem appropriate to use an inversion procedure which, consistent with the dc conductivity, minimizes the interband contribution below $\omega_{\min}$. The procedure is valid if data are available to sufficiently low ω; it should give a good approximation to the Drude parameters if $\omega_{\min}$ is greater than (but close to) the interband absorption threshold, and, in any case, should provide as good an approximation to the Drude absorption as can be obtained from the limited spectral-range reflectivity data.

For the $\omega \to 0$ extrapolation, we used the Drude expression plus a single harmonic-oscillator absorber. The Drude expression for $\hat{\epsilon}(\omega)$ is given by Eq. (8) if $n = 1$, $\omega_j = 0$, $f_j \equiv \omega_p^2$, and $\Gamma_j \equiv 1/\tau_m$, where ω_p and τ_m are the plasma frequency and scattering time, respectively. Thus, for the $\omega \to 0$ extrapolation, we have

$$\hat{\epsilon}(\omega) = 1 - \frac{\omega_p^2 \tau_m}{+\omega^2 \tau_m + i\omega} + \frac{f_2}{(\omega_2^2 - \omega^2) - i\Gamma_2 \omega} . \qquad (11)$$

The extrapolation is thus determined by fixing two Drude parameters, τ_m and

$$\sigma_{dc} = \frac{\omega_p^2 \tau_m}{4\pi} ,$$

as well as the three parameters f_2, ω_2, and Γ_2 of the harmonic-oscillator term. Using $f_2 = 0$ and the bulk σ_{dc} ($4\pi\hbar\sigma_{dc} = 1304$ eV in esu for molybdenum[26]) a trial $\tau_m = 1/\Gamma$ is chosen which yields a calculated $R(\omega)$ somewhat higher than the measured $R(\omega)$ at the lowest energy. This procedure will generate a Drude-type extrapolation function shown as the dotted line (and labeled $FB = 0$) in Fig. 5. Then the parameters f_2, ω_2, and Γ_2 in Eq. (11) are chosen to provide a slope and magnitude match between $R(\omega_{\min})_{calc}$ and $R(\omega_{\min})_{expt}$. The $\omega \to 0$ extrapolation function $R(\omega)$ is then computed using Eqs. (6) and (7), and the data are Kramers-Kronig analyzed. We recall that Drude theory gives[19]

$$\epsilon_2(\omega) = 4\pi\sigma_{dc}/\omega(1 + \omega^2\tau^2) , \qquad (12)$$

$$1 - \epsilon_1(\omega) = 4\pi\sigma_{dc}\tau/(1 + \omega^2\tau^2) , \qquad (13)$$

so that

$$\tau/\hbar = (1 - \epsilon_1)/E\epsilon_2 , \qquad (14)$$

where $E = \hbar\omega$, and from Eq. (12)

$$\tau/\hbar = (1/E)(4\pi\hbar\sigma_{dc}/E\epsilon_2 - 1)^{1/2} . \qquad (15)$$

Thus, for small ω, a calculation of Eq. (14) or (15) from the inverted ϵ_1, ϵ_2 should produce the constant $\tau/\hbar$. We find the surprising result that

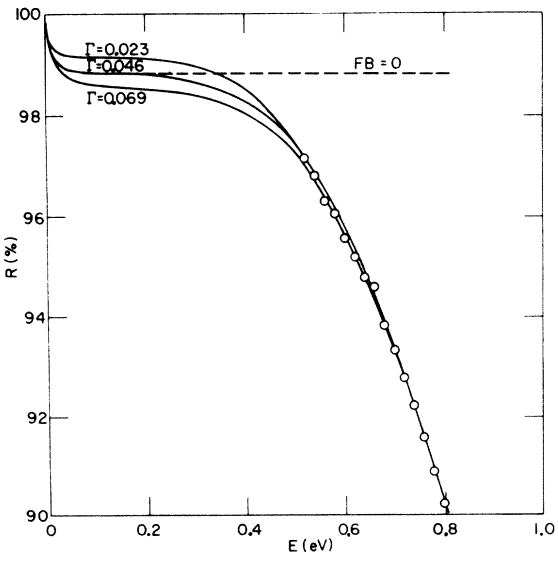

FIG. 5. Extrapolation of the reflectivity from $\omega_{\min}$ to 0. These extrapolations were made with the model functions of Eq. (11) where $\Gamma = 1/\tau_m$. From inspection of this figure alone, there is no obviously preferable extrapolation.

there appears to be a (nearly) unique extrapolation to $\omega = 0$ which leaves $\tau/\hbar$ constant for $\omega < \omega_{min}$ and thus satisfies conditions (a) and (b). Figure 6, for example, shows $\tau/\hbar$ computed with Eq. (14) (solid lines) and from Eq. (15) (dashed lines). The corresponding extrapolations of $R(\omega)$ to $\omega = 0$ are shown in Fig. 5. Clearly, from an inspection of Fig. 5 alone, there is no obviously preferable extrapolation. From Fig. 6, however, we see that (consistent with our extrapolation procedure), only one value of $\tau_m = 1/\Gamma$ will give Drude behavior near ω_{min}. Furthermore, only for this choice of Γ is $\tau/\hbar$ as computed from Eq. (14) equal to that computed from Eq. (15). The behavior of $\tau/\hbar$ (Fig. 6) is essentially independent of the harmonic-oscillator parameters f_2, ω_2, and Γ_2 in Eq. (11) but depends sensitively on the choice of τ_m in Eq. (11). The sensitivity to τ_m enables one to obtain a nearly unique extrapolation. For the optimum extrapolation, $\Gamma = 1/\tau_m = (0.046\ \text{eV})/\hbar$, $f_2 = 28.5$ $(\text{eV}/h)^2$, $\omega_2 = (0.97\ \text{eV})/\hbar$, and $\Gamma_2 = (0.8\ \text{eV})/\hbar$. We emphasize that the accuracy of the optimized reflectivity extrapolation (subject to the limitations mentioned earlier) depends on the accuracy of the reflectivity data. For the data reported here, one is probably not justified in arguing that the $\Gamma = 0.046/\hbar$ extrapolation is more accurate than the other illustrated extrapolations because the uncertainties in the reflectance measurements are too large. However, the procedure for determining an optimum extrapolation function has been demonstrated.

For all extrapolation functions consisting of a sum of harmonic-oscillator and Drude terms, independent of the choice of Γ, the input σ_{dc} is obtained from the Kramers-Kronig inversion. This is expected (although it does not appear to be generally realized) since, as $\omega \to 0$, $\theta(\omega)$ should approach $\theta(\omega)_{Dr}$. (For proof, see Appendix.) This is illustrated in Fig. 7 which shows

$$\frac{\Delta\theta}{\theta} = \frac{\theta_{tot} - \theta_{Dr}}{\theta_{Dr}} ,$$

for the case $\Gamma = 0.046/\hbar$ where θ_{Dr} is calculated from the Drude part of the extrapolation model function and θ_{tot} is the phase from the Kramers-Kronig inversion. For $\omega \gtrsim 0.1$ eV, the interband absorption tail produces a strong upswing in $\Delta\theta/\theta$. Also, below $\sim 10^{-6}$ eV, the function again shows strong divergence indicating that the numerical-inversion procedure has begun to break down. [We found it necessary to go to very low energies ($\sim 10^{-8}$ eV) with a fine integration mesh in order to obtain generally satisfactory convergence of $\Delta\theta/\theta$. For this purpose we use a logarithmic integration mesh.]

As we have seen in Fig. 6, the behavior of $\sigma(\omega)$ from the Kramers-Kronig inversion is not, in general, Drude-like near the low-energy data cutoff. These results are also illustrated in Fig. 8 where we show the way in which $\sigma(\omega)$ for the different extrapolation functions approaches σ_{dc}. Only for $\Gamma = 0.046/\hbar$ is $\sigma(\omega)$ Drude-like. The optimization procedure for the $\omega \to 0$ extrapolation apparently provides a separation of the inverted $\sigma(\omega)$ into a Drude part and an interband part where the interband tailing of $\sigma(\omega)$ below ω_{min} is represented by the harmonic-oscillator term of Eq. (11). The Kramers-Kronig routine will always give back the input Drude parameters at sufficiently low energy, providing that the numerical routines are sufficiently precise (recall that the computation of ϵ_1 comes from

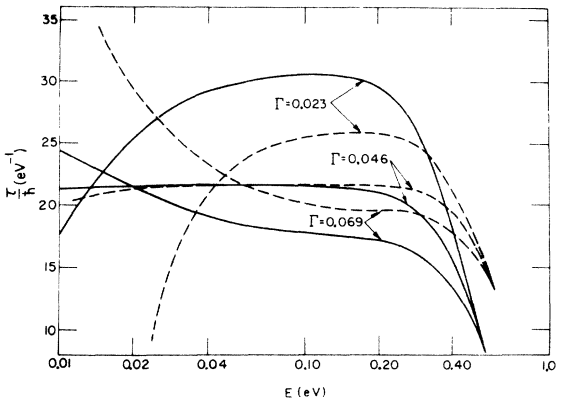

FIG. 6. $\tau/\hbar$ as computed from the inverted ϵ_1, ϵ_2 using the Drude formalism and the $\omega_{min} \to 0$ reflectivity extrapolations shown in Fig. 5. The solid lines were computed from Eq. (14) and the dashed lines from Eq. (15). This figure shows that a nearly unique extrapolation function for the range $0 \le \omega \le \omega_{min}$ can be obtained since only one extrapolation leaves the derived $\tau/\hbar$ constant and hence Drude-like below ω_{min}.

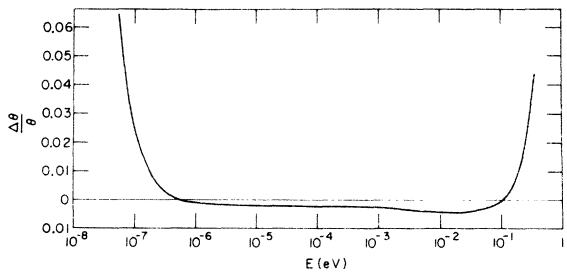

FIG. 7. Phase difference $\Delta\theta/\theta = (\theta_{tot} - \theta_{Dr})/\theta_{Dr}$ vs energy, where θ_{tot} is the Kramers-Kronig inverted result and θ_{Dr} is calculated from the Drude extrapolation model function. As $\omega \to 0$, the inverted phase approaches that of the extrapolation model function; the divergence in $\Delta\theta/\theta$ for $\omega < 10^{-6}$ eV results from breakdown of the numerical integration routine.

$$\epsilon_1 = n^2 - k^2$$

and as $\omega \to 0$, n and k both diverge but the difference ϵ_1 is finite. Thus ϵ_1 represents the relatively small difference between two very large numbers, a numerically difficult situation). Our purpose is thus to maximize the energy range (below ω_{min}) over which the behavior of the inverted optical functions exhibit Drude behavior. It is this requirement which leads to a nearly unique extrapolation function for $R(\omega)$ below ω_{min}.

The optical parameters $\epsilon_1(\omega)$ and $\epsilon_2(\omega)$ below 6 eV, as determined from Kramers-Kronig inversion of the reflectance data with an extrapolation to 25 eV taken from the work of Juenker *et al.*, and with the optimized $\omega \to 0$ extrapolation, are shown in Fig. 9.

The Drude parameters obtained from the analysis of Sec. III are

$$4\pi\hbar\sigma_{dc} = 1304 \text{ eV}$$

(as reported in Ref. 26), and

$$\tau/\hbar = 21 \text{ eV}^{-1}.$$

With σ_{dc} as input, the latter parameter was derived from reflectivity data taken for $\hbar\omega \geq 0.5$ eV. $\tau/\hbar$ reported here agrees well with the value of 18 eV^{-1} reported by Kirillova *et al.*[1] which was derived from infrared measurements between 0.06 and 0.15 eV (Kirillova's analysis yields a value of $\sigma_{dc} \simeq 0.5$ of the bulk value, however).

Since the Drude parameters are now determined, we can extract the free-electron contribution from the total $\sigma(\omega)$ to obtain $\sigma_{interband}$ (this requires the assumption that τ is frequency independent). Subsequent figures (paper II) will show only the interband contribution to $\sigma(\omega)$.

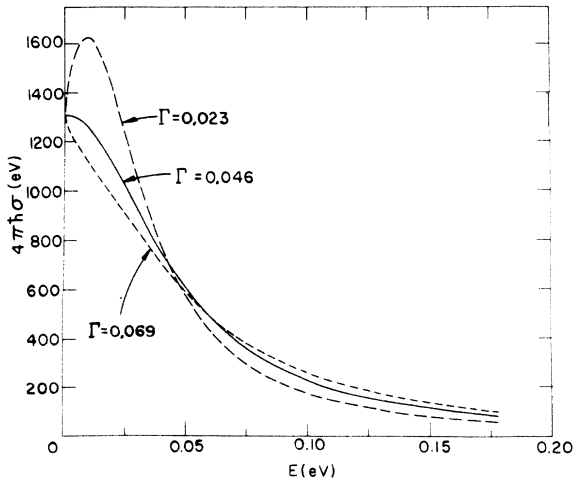

FIG. 8. Frequency-dependent conductivity for $\omega < \omega_{min}$ obtained from the three extrapolation functions shown in Fig. 5. Whereas, in each of these curves, $\sigma \to \sigma_{dc}$ as $\omega \to 0$, only the solid line has Drude-like behavior.

IV. SUM RULES

Evaluating the well-known sum rule[27]

$$n_{eff}(\omega) = \frac{2}{\pi}\left(\frac{m}{4\pi Ne^2}\right)\int_0^{\omega} \omega'\epsilon_2(\omega')\,d\omega' \tag{16}$$

(where N is the atom density, m is the free-electron mass), which is a measure of the number of electrons available for excitation by a photon of energy $\hbar\omega$, we obtain the reasonable result that $n_{eff} = 5.2$ at 25 eV indicating that the oscillator strength of the six valence electrons in molybdenum (atomic configuration d^5s^1) is nearly exhausted at this energy (no contribution to n_{eff} attributable to transitions from outer-lying electronic levels of the krypton core would be expected for $E < 25$ eV[28]). This result differs appreciably from the value of approximately 7 (at 25 eV) deduced by Juenker *et al.*[5]

In addition, the sum rules

$$\int_0^{\infty} [n(\omega') - 1]\,d\omega' = 0, \tag{17}$$

$$\int_0^{\infty} [1 - \epsilon_1(\omega')]\,d\omega' = (2\pi^2)\sigma_{dc}, \tag{18}$$

have recently been reported by Altarelli *et al.*[29] These sum rules, when expressed as

$$f(E) = \int_0^{E} [n(E') - 1]\,dE', \tag{19}$$

$$g(E) = \frac{2}{\pi}\int_0^{E} [1 - \epsilon_1(E')]\,dE', \tag{20}$$

provide tests of the numerical accuracy of the Kramers-Kronig inversion routines. Figures 10

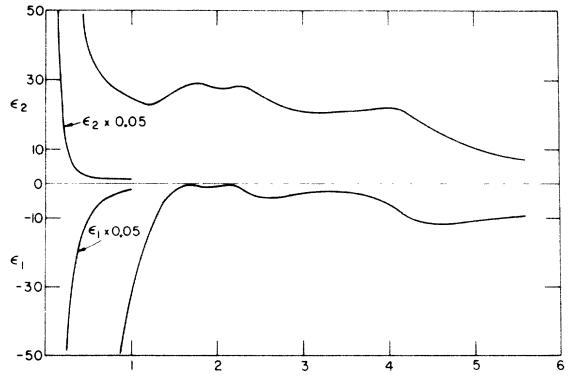

FIG. 9. Real and imaginary components of $\hat{\epsilon}(\omega)$ for molybdenum from Kramers-Kronig inversion of the reflectance data.

and 11 show the functions $f(\omega)$ and $g(\omega)$, both of which apparently satisfy the sum rules given by Eqs. (17) and (18). These sum rules thus provide additional evidence that the inversion routines are satisfactory.

We notice that both of the functions $f(\omega)$ and $g(\omega)$ are heavily weighted by the Drude region of the spectrum. When $\hbar\omega = \hbar\omega_{\min} = 0.5$ eV, each of these functions has reached 50%, or more, of its maximum value with a substantial contribution coming from the region $\hbar\omega < 0.01$ eV. The sum rules thus provide tests of the numerical accuracy of the inversion routines, particularly as the routines are affected by the extrapolation $\hbar\omega \to 0$.

V. CONCLUSIONS

The near-normal-incidence reflectivity of molybdenum has been measured between 0.5 and 6 eV. New analytical procedures are reported for performing the Kramers-Kronig inversions. Using the dc conductivity as input, a procedure is described for the $\omega \to 0$ extrapolation which permits one to extract the Drude parameter τ in a (nearly) unique fashion. Sum rules computed include the well-known "f sum rule," as well as recently reported integrals which serve as useful tests of the numerical-inversion routines. An estimated intraband contribution (based on the derived Drude parameters) is extracted from the measured $\sigma_{\text{tot}}(\omega)$ for comparison with the corresponding theoretical quantity discussed in the subsequent paper.

APPENDIX

We wish to show that the Kramers-Kronig inversion of reflectance data extrapolated from $\omega_{\min}$ to 0 with a Drude function must yield the input Drude functions $\epsilon_1(\omega)$ and $\epsilon_2(\omega)$ at sufficiently low ω; i.e., the inverted phase $\theta_{\text{tot}}(\omega)$ must approach the Drude phase $\theta_{\text{Dr}}(\omega)$ as $\omega \to 0$.

With the assumption that Drude theory describes optical absorption at sufficiently low energies in a metal, it follows that the complex dielectric function of the metal can be represented as

$$\hat{\epsilon} = 1 - \frac{4\pi\sigma_{\text{dc}}}{+\omega^2\tau + i\omega} + \sum_{i=1}^{n} \frac{f_i}{(\omega_i^2 - \omega^2) - i\Gamma_i\omega}\,, \tag{A1}$$

namely, as the sum of a single Drude term and some number n of harmonic-oscillator absorbers with parameters f_i, ω_i, and Γ_i appropriately chosen.[22,30] It may be that τ is a frequency-dependent parameter, but one might expect this dependence to be small near $\omega = 0$ so that the Drude formalism would be appropriate in this regime. For higher energies, the representation given above is valid.

Recall that the phase is related to $\hat{r}$ through the definition

$$\hat{r} = \sqrt{(R)}e^{i\theta}\,, \tag{A2}$$

so that

$$\theta = \text{Arc tan}\left(\frac{\text{Im}\,\hat{r}}{\text{Re}\,\hat{r}}\right). \tag{A3}$$

To evaluate $\hat{r}$, we use Fresnel's relation

$$\hat{r} = \frac{\hat{n} - 1}{\hat{n} + 1}\,, \quad \hat{\epsilon} = (\hat{n})^2\,, \quad \hat{n} = n + ik\,, \tag{A4}$$

with $\hat{\epsilon}$ expressed as

$$\hat{\epsilon} = |\hat{\epsilon}|e^{i\alpha} \equiv \epsilon_1 + i\epsilon_2\,. \tag{A5}$$

Algebraic manipulation yields the result

$$\theta = \tan^{-1}\beta; \quad \beta = \frac{[2(|\hat{\epsilon}|^2 - \text{Re}\,\hat{\epsilon})]^{1/2}}{|\hat{\epsilon}|^{1/2}(|\hat{\epsilon}| - 1)}\,. \tag{A6}$$

From Eq. (A1), we obtain

$$\text{Re}\,\hat{\epsilon} = \left(1 - \frac{4\pi\sigma_{\text{dc}}\tau}{1 + \omega^2\tau^2}\right) + \sum_i \frac{f_i(\omega_i^2 - \omega^2)}{(\omega_i^2 - \omega^2)^2 + \Gamma_i^2\omega^2}\,, \tag{A7}$$

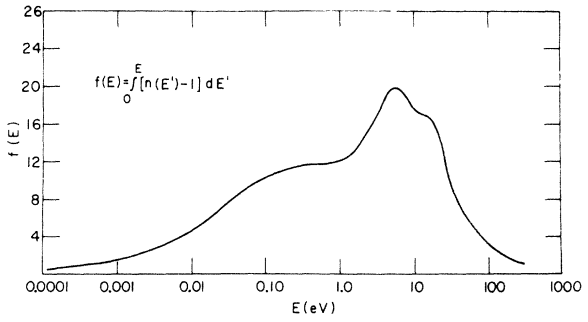

FIG. 10. Sum rule $f(E) = \int_0^E [n(E') - 1]\,dE'$ (see Ref. 29) calculated from the refractive index obtained by Kramers-Kronig inversion of the molybdenum reflectance data. For large E, $f(E) \to 0$.

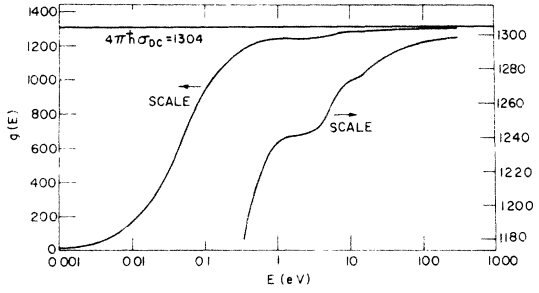

FIG. 11. The sum rule $g(E) = (2/\pi)\int_0^E [1 - \epsilon_1(E')]dE'$ (see Ref. 29) for molybdenum. As E becomes large, $g(E) \to 4\pi\hbar\sigma_{\text{dc}}$. This sum rule and that of Fig. 10 provide tests of the numerical accuracy of the inversion procedure.

$$\mathrm{Im}\hat{\epsilon} = \left(\frac{4\pi\sigma_{dc}}{\omega(1+\omega^2\tau^2)} + \sum_i \frac{f_i\Gamma_i\omega}{(\omega_i^2-\omega^2)^2+\Gamma_i^2\omega^2}\right). \tag{A8}$$

We now perform a series of expansions and list the coefficients needed to get the first-order term of $(\theta_{tot}/\theta_{Dr})$ in a power series in ω.

$$\mathrm{Re}\hat{\epsilon} = C_0 + C_2\omega^2 + C_4\omega^4 + \cdots; \quad C_0 = 1 - 4\pi\sigma_{dc}\tau + f_i/\omega_i^2, \tag{A9}$$

$$\mathrm{Im}\hat{\epsilon} = B_0/\omega + B_1\omega + B_3\omega^3 + \cdots;$$

$$B_0 = 4\pi\sigma_{dc}, \quad B_1 = (4\pi\sigma_{dc}\tau^2 + f_i\Gamma_i/\omega_i^4), \tag{A10}$$

$$|\hat{\epsilon}|^2 = (\mathrm{Re}\hat{\epsilon})^2 + (\mathrm{Im}\hat{\epsilon})^2 = (1/\omega^2)(F_0 + F_2\omega^2 + F_4\omega^2 + \cdots);$$

$$F_0 = B_0^2, \quad F_2 = C_0^2 + 2B_0B_1, \tag{A11}$$

$$|\hat{\epsilon}|^{1/2} = \pm\omega^{-1/2}(h_0 + h_2\omega^2 + h_4\omega^4 + \cdots); \quad h_0 = F_0^{1/4},$$

$$h_2 = \tfrac{1}{4}F_0^{-3/4}F_2, \tag{A12}$$

$$|\hat{\epsilon}| - 1 = (h_0^2/\omega)(1 + g_1\omega + g_2\omega^2 + g_4\omega^4 + g_6\omega^6 + \cdots);$$

$$g_1 = -1/h_0^2, \quad g_2 = 2h_2/h_0. \tag{A13}$$

Combining Eqs. (A9)–(A13) with Eq. (A6), keeping terms to order $\omega^{5/2}$, we obtain

$$\beta = \frac{(2\omega)^{1/2}}{h_0}(1 + \xi_1\omega + \xi_2\omega^2 + \cdots);$$

$$\xi_1 = g_1, \quad \xi_2 = C_0/2F_0 + h_2/h_0 - g_2 - g_1^2. \tag{A14}$$

The final expansion yields

$$\theta_{tot} = \tan^{-1}\beta = (p_1\omega^{1/2} + p_3\omega^{3/2} + p_5\omega^{5/2} + \cdots); \quad p_1 = \frac{2}{2\pi\sigma_{dc}}, \quad p_3 = -\frac{5}{12\pi\sigma_{dc}}\left(\frac{2}{4\pi\sigma_{dc}}\right)^{1/2},$$

$$p_5 = \frac{1}{(4\pi\sigma_{dc})^2}\left(\frac{2}{4\pi\sigma_{dc}}\right)^{1/2}\left[-1.95 + 4\pi\sigma_{dc}\tau + \frac{(4\pi\sigma_{dc}\tau)^2}{4} - \left(\frac{f_i}{\omega_i^2}\right)(1 - 4\pi\sigma_{dc}\tau) - \frac{1}{4}\left(\frac{f_i}{\omega_i^2}\right)^2\left(1 + \frac{8\pi\sigma_{dc}\Gamma_i}{f_i}\right)\right], \tag{A15}$$

where θ_{tot} represents the phase of a real metal.

We have $\theta_{tot}(\omega) \to 0$ as $\omega \to 0$ as expected. The Drude phase θ_{Dr} is the same as θ_{tot} except $f_i = 0$, thus

$$\theta_{Dr} = q_1\omega^{1/2} + q_3\omega^{3/2} + q_5\omega^{5/2} + \cdots; \quad q_1 = p_1, \quad q_3 = p_3, \quad q_5 = p_5 \ (\text{with } f_i = 0), \tag{A16}$$

so that

$$\frac{\theta_{tot}}{\theta_{Dr}} = 1 + k_2\omega^2 + \cdots,$$

$$k_2 = \frac{p_5 - q_5}{p_1} = \frac{1}{(4\pi\sigma_{dc})^2}\sum_i \left[-\left(\frac{f_i}{\omega_i^2}\right)(1 - 4\pi\sigma_{dc}\tau) - \frac{1}{4}\left(\frac{f_i}{\omega_i^2}\right)^2\left(1 + \frac{8\pi\sigma_{dc}\Gamma_i}{f_i}\right)\right],$$

and hence $\theta_{tot}/\theta_{Dr} \to 1$ as $\omega \to 0$. Q. E. D.

*Work performed under the auspices of the U. S. Atomic Energy Commission.

[1]M. M. Kirillova, L. V. Nomerovannaya, and M. M. Noskov, Zh. Eksp. Teor. Fiz. 60, 2252 (1971) [Sov. Phys.—JETP 33, 1210 (1971)].

[2]M. M. Kirillova, G. A. Bolotin, and V. M. Mayevsky, Fiz. Met. Metalloved. 24, 95 (1967) [Phys. Met. Metallogr. 24, 91 (1967)].

[3]M. M. Kirillova and B. A. Charikov, Fiz. Met. Metalloved 19, 495 (1965) [Phys. Met. Metallogr. 19, 13 (1965)].

[4]J. P. Waldron and D. W. Juenker, J. Opt. Soc. Am. 54, 204 (1964).

[5]D. W. Juenker, L. B. LeBlanc, and C. R. Martin, J. Opt. Soc. Am. 58, 164 (1968).

[6]J. H. Weaver, Ph.D. thesis (Iowa State University, Ames, Iowa, 1973) (unpublished).

[7]Yu. P. Udoev, N. S. Kozyakova, and M. L. Kapitza, Fiz. Met. Metalloved 31, 439 (1971) [Phys. Met. Metallogr. 31, 227 (1971)].

[8]G. A. Bolotin, V. M. Mayevskiy, and B. A. Charikov, Fiz. Met. Metalloved 25, 629 (1968) [Phys. Met. Metallogr. 25, 49 (1968)].

[9]A. P. Lenham and D. M. Treherne, in *Optical Properties and Electronic Structure of Metals and Alloys*, edited by F. Abeles (North-Holland, Amsterdam, 1966), p. 196.

[10]A. P. Lenham and D. M. Treherne, J. Opt, Soc. Am. 56, 1137 (1966).

[11]K. A. Kress and G. J. Lapeyre, in *Electronic Density of States*, NBS Publ. No. 323, edited by L. H. Bennett (U.S. GPO, Washington, D.C., 1971), p. 209.

[12]Kenneth A. Kress and Gerald Lapeyre, J. Opt. Soc. Am. 60, 1681 (1970).

[13]M. L. Kapitza, Yu. P. Odoev, and E. I. Shirokikh, Fiz. Tverd. Tela 11, 816 (1969) [Sov. Phys.-Solid State 11, 665 (1969)].

[14]J. B. Sabine, Phys. Rev. 55, 1064 (1939).

[15]J. Anderson, G. W. Rubloff, and P. J. Stiles, Solid State Commun. 12, 825 (1973).
[16]B. W. Veal, F. M. Mueller, R. Afshar, and J. Shaffer, AIP Conf. Proc. 5, 1285 (1972).
[17]See J. G. Endriz and W. E. Spicer, Phys. Rev. B 4, 4144 (1971) and references cited therein.
[18]J. M. Elson and R. H. Ritchie, Phys. Lett. A 33, 255 (1970).
[19]F. Seitz, *The Modern Theory of Solids* (McGraw-Hill, New York, 1940), Chap. XVII.
[20]E. L. Kreiger, D. J. Olechna, and D. S. Story (unpublished).
[21]H. R. Philipp and H. Ehrenreich, J. Appl. Phys. 35, 1416 (1964).
[22]Hans W. Verleur, J. Opt. Soc. Am. 58, 1356 (1968).
[23]R. Afshar, F. M. Mueller, and J. C. Shaffer, J. Comp. Phys. 11, 190 (1973).
[24]J. C. Shaffer, B. Van Pelt, C. Wood, J. Freeouf, K. Murase, and J. W. Osmun, Phys. Status Solidi 54, 511 (1972).
[25]H. E. Bennett, J. M. Bennett, E. J. Ashley, and R. J. Motyka, Phys. Rev. 165, 755 (1968).
[26]*Handbook of Chemistry and Physics*, 40th ed. (Chemical Rubber, Cleveland, Ohio, 1958), p. 2590.
[27]H. Ehrenreich, in *Optical Properties of Solids*, edited by J. Tauc (Academic, New York, 1966), p. 106.
[28]K. Siegbahn, C. Nordling, A. Fahlman, R. Nordberg, K. Hamrin, J. Hedman, G. Johansson, T. Bergmark, S. Karlsson, I. Lindgren, and B. Lindberg, ESCA *Atomic, Molecular, and Solid State Structure Studied by Means of Electron Spectroscopy* (Almquist and Wiksells, Uppsala, Sweden, 1967), p. 226.
[29]M. Altarelli, D. L. Dexter, H. M. Nussenzveig, and D. Y. Smith, Phys. Rev. B 6, 4502 (1972).
[30]M. Cardona, in *Optical Properties of Solids*, edited by S. Nudelman and S. S. Mitra (Plenum, New York, 1969).